Magnetic behaviour in metal-free radical thin films

Tobias Junghoefer,[1,6] Arrigo Calzolari,[2,6] Ivan Baev,[3,6] Mathias Glaser,[1] Francesca Ciccullo,[1] Erika Giangrisostomi,[4] Ruslan Ovsyannikov,[4,] Fridtjof Kielgast,[3] Matz Nissen,[3] Julius Schwarz,[3] Nolan M. Gallagher,[5] Andrzej Rajca,[5] Michael Martins,[3] Maria Benedetta Casu[1,7*]

[1]Institute of Physical and Theoretical Chemistry, University of Tübingen, 72076 Tübingen, Germany

[2]CNR-NANO Istituto Nanoscienze, Centro S3, 41125 Modena, Italy

[3]Department of Physics, University of Hamburg, 22761 Hamburg, Germany

[4]Helmholtz-Zentrum Berlin, 12489 Berlin, Germany

[5]Department of Chemistry, University of Nebraska, Lincoln, United States

[6]These authors contributed equally

[7] Lead contact

*benedetta.casu@uni-tuebingen.de

SUMMARY

Magnetism in organic materials is very intriguing: the realization of long-range magnetic order in completely metal-free systems combines magnetic moments with useful properties of organic materials, such as optical transparency, low-cost fabrication, and flexible chemical design. An essential step for application is the knowledge of the magnetic behaviour that, so far, was investigated only in the proximity of light atoms to heavy metals, impurities, or vacancies, and not as an intrinsic property of thin films that are purely organic. Here, we unravel X-ray magnetic circular dichroism at the carbon and nitrogen K-edges in purely organic radical thin films. Our results show that, controlling the preparation, the magnetic behaviour is different than in single crystals. Atomistic simulations indicate that the reason for this is the molecular arrangement in the films when compared to that in the single crystal. The tuning of the film

magnetic properties by the molecular arrangement is an exciting perspective towards revealing new properties and applications.

KEYWORDS: Organic radicals, magnetism, X-ray magnetic circular dichroism, ab initio calculations

INTRODUCTION

Magnetic ordering in thin films of light elements, such as nitrogen and carbon, is an intriguing characteristic of matter that is mostly unknown. It has been studied in magnetic-edged graphene nanoribbons[1] or bilayers[2], and polymers[3] while in organic thin films most of the investigations show this effect as due to the proximity of light atoms to heavy metals, impurities, or vacancies[4]. Conversely, purely organic radicals are molecules that carry one unpaired electron giving rise to a permanent magnetic moment, in the complete absence of metal ions, impurities or vacancies.[5-7] They are exceptionally promising in various fields ranging from quantum computing to organic spintronics.[8-12] Consequently, the need arose to go beyond the initial attempts to grow films by wet preparation that is prone to the presence of contaminants. The controlled growth of radical thin film using evaporation was believed not practicable because of their reactivity that would cause irreversible degradation during evaporation.[13] Once proved that several families of radicals are stable enough to be evaporated,[14] the perspective of potential applications are driving the research on their thin film,[9-11,15,16] which is the necessary phase for any realistic application. Inspired by their tremendous potential, here we investigate thin films of an exceptionally chemically stable Blatter radical derivative,[17] a small molecular compound, by using X-ray magnetic circular dichroism (XMCD).[18-21] Here we observe for the first time XMCD at the nitrogen and carbon K-edges: our results show a magnetic behaviour different

than in the single crystals depending on the preparation conditions. First principles investigations support these findings and provide a microscopic explanation of the variability of the long-range magnetic properties of radical thin films.

RESULTS AND DISCUSSION

Several technical, methodological, and theoretical challenges must be overcome to investigate the magnetic behaviour of radical thin films. While several radicals are synthetized with high enough chemical stability to stand evaporation, their film forming properties are often very poor. This depends on their high vapor pressure at room temperature and their low molecular weight that make them highly volatile and characterized by very low sticking coefficients.[17,22] To achieve reproducible films and, thus, reproducible results, controlled conditions during growth are necessary to avoid any artefacts (contaminants, degradation due to film aging and air-exposure). The investigations require high signal sensitivity: a single magnetic moment is associated with a large molecular volume. The high sensitivity is furthermore necessary because we investigate very thin films (the nominal thickness varies in the 4-9 nm range). An important issue is also achieving very low temperature in the presence of high magnetic fields to reach magnetic saturation. In fact, purely organic radicals are predicted to have low Curie temperatures;[5-7,23,24] and no previous knowledge on the behaviour of the thin films and their dynamics[24] is at hand. Thus, it was necessary to have a setup that allows scanning a large temperature range, including very low temperatures. Considering these aspects, we adopted two strategies. i) We selected a chemically stable Blatter radical[25,26] derivative, (Blatter-pyr, Figure 1a)[17] explicitly designed to have very good film forming properties and film stability.[17] ii) XMCD was the experimental technique of our choice. It is an element-specific technique based on the absorption of polarized X-rays due to electron transitions from core levels to unoccupied states, a well-established method to access spin and orbital angular momenta in transition metals, identifying their magnetic behaviour.[18-21] Despite the XMCD well-known capabilities, the

measurements of metal-free organic films require exceptional facilities. The experiments were performed using a newly developed ultra-low temperature setup equipped with a superconducting vector magnet allowing magnetic fields up to ±7 T in the horizontal direction and ±0.5 T in the vertical direction, and a cryogen free ^{3}He-^{4}He dilution refrigerator, allowing experiments reaching the lowest temperature of 100 mK.[27] This unique portable setup features an ultra-high vacuum (UHV) preparation chamber that allowed growing the radical films by organic molecular beam deposition under controlled conditions, and transferring them to the measuring chamber without breaking the UHV. This led to the investigation of thin films free from contaminants because catalysts, solvents and air exposure may affect the intrinsic film properties.

We applied a magnetic field at very low temperature, to align the magnetic moments in the direction of the field that was collinear to the incoming circularly polarized photon beam. The absorption spectra (XAS) once with left and once with right circularly polarized light were measured (Figure 1b).

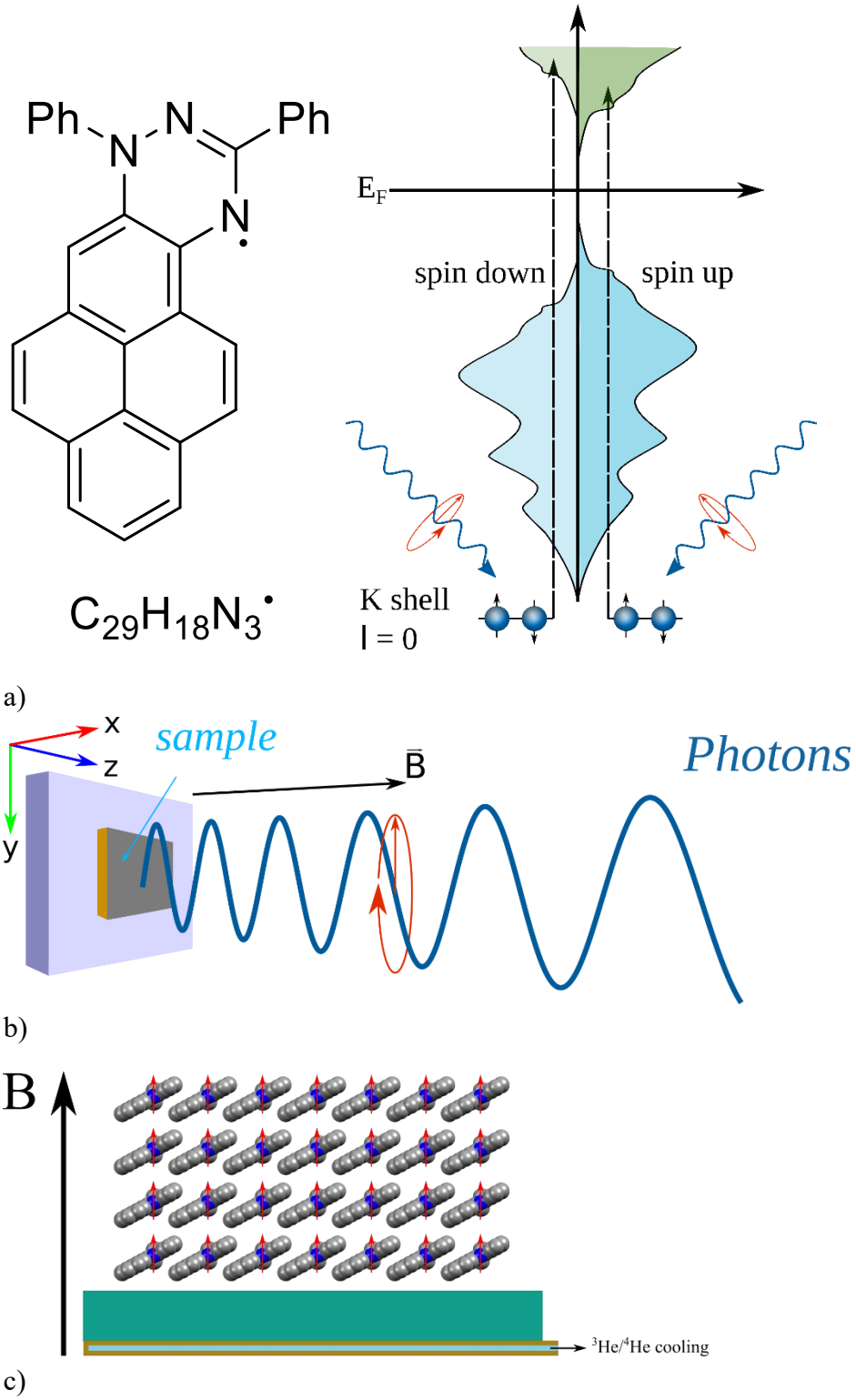

Figure 1. Molecular structure of the pyrene Blatter derivative and experiment. a. (left panel) Molecular structure. (right panel) XMCD principles in a one-electron model. Electron transitions from core levels to unoccupied states occur due to absorption of circularly

polarised X-rays The absorption spectra are measured once with left and once with right circularly polarized light **b**. Sketch of the geometry of the experiment: . **c**. A magnetic field at very low temperature aligns the radical magnetic moments in the direction of the field. The direction of the magnetic field and the incoming polarised light are collinear.

XMCD is defined as the difference between the two absorption signals. We focus on the N K-edge absorption spectra measured at 1.1 K with a magnetic field of +7 T. The films in Figure 2 (nominal thickness 9 nm) were prepared by using controlled evaporation keeping the substrate at 290 K. We observe a clear dichroic signal (Figure 2). The signal reverses sign upon reversal of the magnetic field (Supporting Information, Figure S1) confirming that the dichroism is real (magnetization reversal is equivalent to switching the helicity of the polarized light). We also measured the absorption at the C K-edge: a XMCD signal is visible also in this case. This behaviour is surprising because the Blatter-pyr single crystal is antiferromagnetic,[28] in which case no XMCD should be observable. Differences in the intensity of the XMCD for the two signs of the magnetic field suggest the presence of uncompensated spins that do not follow the external magnetic field.[29-31] Also, the curves are normalized considering the total absorption of the beamline (see the experimental section for details), as it is usually done for XMCD.[19,32,33] This method cannot compensate for possible substrate contaminants contributing to absorption.

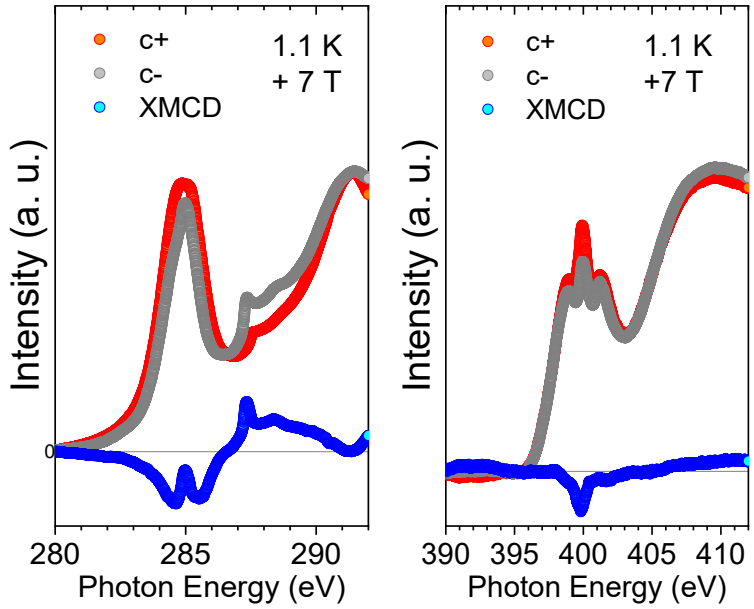

Figure 2. X-ray absorption measurements. Circularly polarized (left) C K-edge and (right) N K-edge XAS for left and right polarisations (c+ and c-) and XMCD, as indicated, recorded in normal incidence at B=7 T, at 1.1 K (substrate temperature during preparation at 290 K, nominal thickness 9 nm).

Uncompensated spins, i.e., spins that are anchored in antiferromagnetic materials and do not follow an applied external field, have been previously observed in inorganic materials, in their thin films or at their interfaces.[29,34-37] To understand the origin of this unexpected behaviour we deposited and investigated a second set of Blatter-pyr thin films with different thicknesses (4 and 9 nm, the latter as in the measurements in Figure 2), at 0.15, 10 and 15 K to span a larger temperature range. We prepared the samples keeping the substrate temperature slightly higher (300 K). This increased the kinetic energy of the Blatter-pyr on the substrate during film growth.[17] We measured the X-ray absorption spectra of the films as previously done and we could not detect any XMCD (Figure 3). Also, we did not detect any dichroism spanning a large

temperature range from 0.15 to 15 K. This result is concomitant with the antiferromagnetic behaviour of the Blatter-pyr crystalline bulk. Therefore, we found that, depending on the growth conditions, either the samples resemble the bulk character, or they have a spin-uncompensated magnetic behaviour.

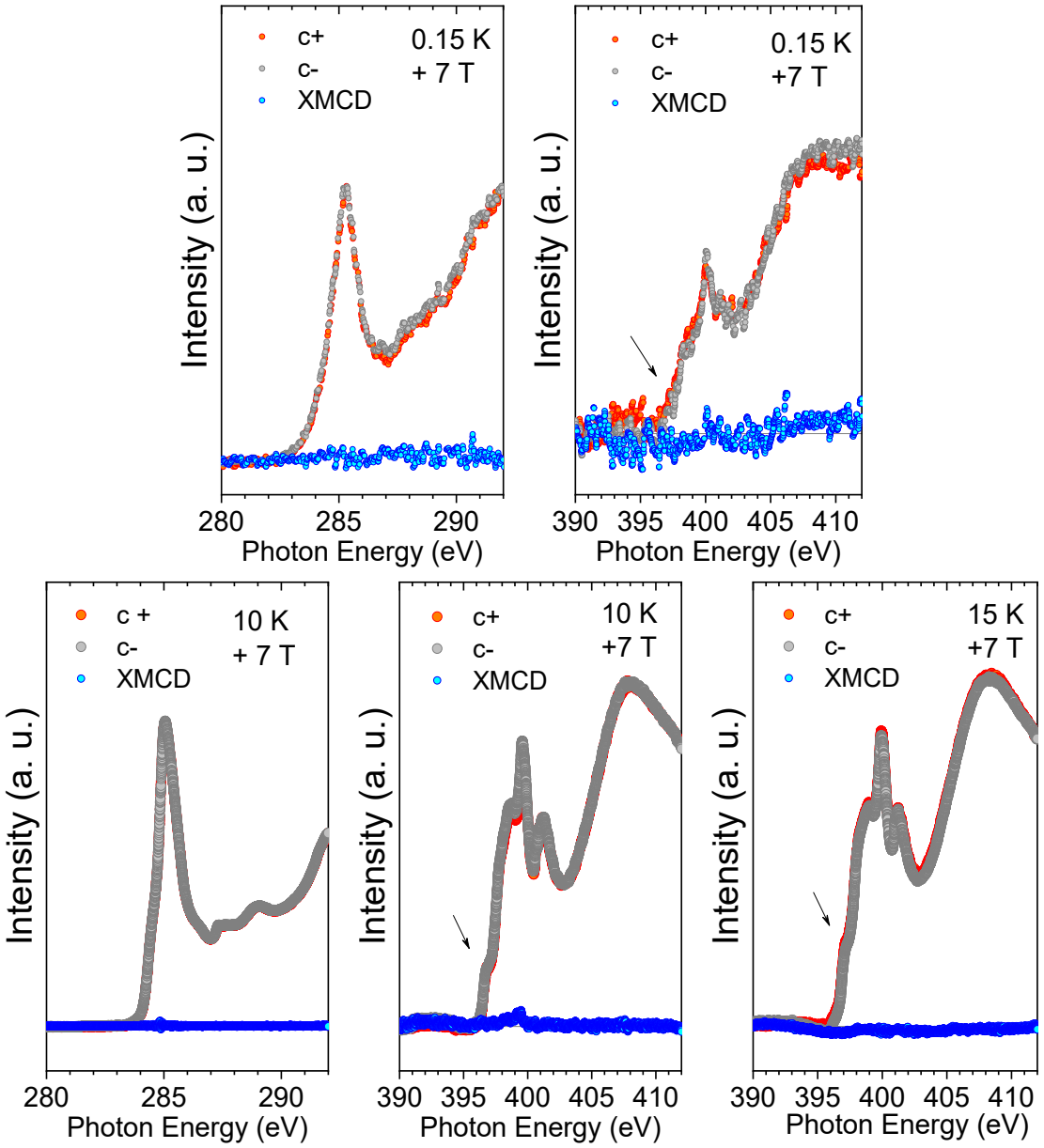

Figure 3. X-ray absorption measurements. Circularly polarized C K-edge and N K-edge XAS for left and right polarisations (c+ and c-) and XMCD recorded in normal incidence at B=7 T, and temperature as indicated (substrate temperature during preparation at 300 K,

nominal thickness 4 (upper panel) and 9 nm (lower panel)). The spectra at 0.15 K were measured with lower resolution. The features are therefore less resolved than at 10 K but still present (see also Supporting information, Figure S3).

Not only do the different preparation conditions cause a different XMCD, but also the presence of a new feature at the N K-edge (Figure 3, and S3 in the Supporting Information) when the samples are grown on the substrate at 300 K. This is an indication of differences in the electronic structure, expected when a different molecular arrangement occurs (see also the calculations below).[38,39]

Thin films can have considerably different structural, transport, electronic and magnetic properties with respect to their bulk counterpart.[40,41] Additionally, molecules have 3N degrees of freedom with N being the number of atoms in a molecule. This has pronounced consequences for all properties of the system. For example, molecular packing has been invoked to explain the different magnetic behaviour ranging from antiferro- to ferromagnetic[23,42] in the different crystallographic phases of the crystals of the first purely organic ferromagnet ever reported, the *p*-nitrophenyl nitronyl nitroxide radical.[7] A widely investigated method to change the molecular orientation in thin films of the same material is tuning the preparation conditions.[43] In our experiments we observe that different preparation conditions play a role. Decreasing the kinetic energy of the molecules on the substrates influences their adjustment in the films[40,44,45] with clear consequences on the magnetic interactions because the antiferromagnetic character of the Blatter-pyr crystals depends on a delicate adjustment of the slippage angle.[28,46]

Energetically, the antiferro- (AF) and the ferromagnetic (FM) interactions in the bulk are very close: we performed first-principles density functional theory calculations for the Blatter-pyr derivative that indicate that the antiferromagnetic configuration is more stable by only ~2 meV/cell. The electronic and magnetic properties of the crystalline bulk along with those of the

single Blatter-pyr molecule are summarized in the Supporting Information (Figure S4 and S5). The minimization of the electronic problem for a non-magnetic state (para or diamagnetic) does not converge to a minimum, that means that the zero magnetization is not a (either total or local) minimum for the total energy, indicating that the non-magnetic phase is not the ground state for the system.

To shed light on the correlation between molecular arrangement, induced by different preparations, and the intermolecular interactions, we have modelled the thin films. Starting from the bulk crystalline structure[17] (Figure 4a), we considered a 9 nm-thick film grown along the *c*-axis, as shown in Figure 4b. The film structure stems from the stacking of the four radicals (labelled 1-4 in the following analysis), which form the crystal. As for the crystalline case, the AF and the FM interactions are almost energetically degenerate. Hereafter, we assume the AF as the reference.

The total magnetic moment of the antiferromagnetic case is the sum of the single molecule contributions with antiparallel spin orientation. The antiparallel magnetic arrangement can be distinguished by the non-magnetic spin unpolarized case, through the evaluation of the absolute magnetization $\mu_A = \int |\rho_{up} - \rho_{dw}| d^3r$, where ρ_{up}-ρ_{dw} are the spin-up and spin-down charge density, respectively. Non-magnetic systems have $\mu_T = \mu_A = 0$, while antiparallel spin systems have $\mu_T = 0$ and $\mu_A \neq 0$. In the present case μ_T=0.0 and μ_A=15.2 Bohr magneton (μ_B)/cell. The spin alternation follows the structural bi-layer arrangement (↑↑ - ↓↓): spin-up for molecules 2 and 3, spin-down for 1 and 4, as shown by the charge spin-density plot (i.e., ρ_{up}-ρ_{dw}) in Figure 4a, where green and blue lobes represent the spin-up and spin-down orientation, respectively. The charge spin density reflects the existing unpaired spin-up/spin-down electronic states. This is explicitly shown in the density of states (DOS, Figure 4b) that closely derives from the coherent superposition of the molecular spectra, where each radical exhibits an unpaired singly occupied (SOMO, S_O) and singly unoccupied (SUMO, S_U) molecular orbital.[47] For molecules

2-3, S_O and S_U have spin-up and spin-down polarization, respectively, while the opposite order attains for molecules 1-4. The electronic and magnetic properties of the film do not depend on the molecular orientation of the external layers (see Supporting Information, Figure S6a). Similar results can be obtained also for the films grown along the *a*- and *b*-axis respectively, see, e.g., Figures S6 b and c.

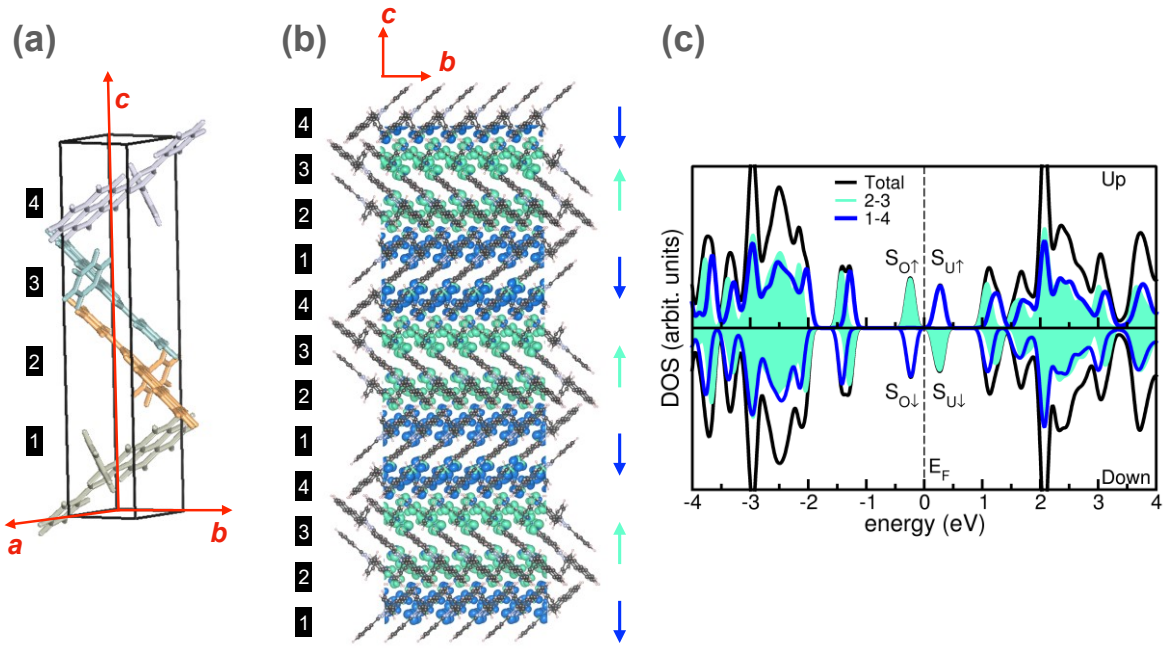

Figure 4. Calculation results for the Blatter-pyr antiferromagnetic film. a. Primitive cell of monoclinic Blatter-pyr crystal. Labels 1-4 indicate the four molecules in the cell. **b.** Side view of the 9 nm-thick film. Coloured isosurfaces represent the charge spin-density plots for the antiferromagnetic phase. Green (blue) colour indicates the majority (minority) spin-up (spin-down) orientation of single radicals. Atomic positions and charge spin-density have been replicated for clarity. **c.** Total and molecule projected spin-polarized density of states. Total (black line) and molecule projected (shaded green areas for molecules 2-3 and thick blue line for molecules 1-4) spin-polarized density of states (DOS) of the Blatter-pyr film. Vertical dashed line marks the Fermi level of the system assumed as energy reference for the plot. S_O (S_U) indicate the single occupied (unoccupied) molecular orbitals for the spin up (↑) and spin down (↓) channels.

A closer inspection of the electronic properties indicates that, albeit weak, there is a long-range intermolecular coupling in the film. This is evident, e.g., from the band structure (Supporting Information, Figure S7a): (i) the molecular-derived bands are not fully degenerate, but rather split in a 2-fold manifolds; (ii) the S_O and S_U bands have k-dispersion of ~100 meV across the Brillouin zone. S_O and S_U states, which are responsible for the magnetic character of the radical, are π-orbitals with a net contribution from both carbon and nitrogen atoms. Even though the magnetic origin of the radical is formally due to the presence of an undercoordinated N atom, the spin-density distribution (i.e., ρ_{up}-ρ_{dw}) is spatially delocalized all over the molecule and not centred on the nitrogen site.[8] Near edge X-ray absorption fine structure (NEXAFS) spectra mirror this delocalization (see Supplemental Information Figure S8). This also explains the reason why we simultaneously observed a XMCD signal at the N and C K-edges in the films (Figure 2).

To unravel the interplay between the molecular orientation and the magnetic character we consider a simple model consisting of a 3 nm-thick film, resulting from the stacking of the four molecules 1-4 (Figure 5a). Starting from the bulk-like arrangement (θ=0°) we modified the molecular orientation by changing the herringbone angle by 5°, 10°, 15° and 20°, with respect to the *c*-axis. The higher is the rotation angle the flatter is the molecular stacking. This mimics the interaction of the molecules with the colder substrate that results in a reduced mobility and a more flat lying molecular arrangement.[48-50] After full atomic relaxation, we recognize different configurations as a function of the initial angles. For θ≤10°, the system maintains the structural and electronic characteristics of the 9 nm-thick films and the crystalline bulk, both AF and FM interactions can be obtained at the same energy. For θ≥15°, the molecule-molecule interaction becomes predominant, and the structure undergoes a strong spatial redistribution, as

shown in Figure 5b for the case of θ=20°. The external molecules 1 and 4 slightly displace from the centre of the film and rotate back restoring the crystalline (θ=0°) spatial distribution. The internal molecules 2-3 rotate in the opposite direction (i.e., increasing θ) forming a close-packed bi-layer of parallel molecules. The resulting configuration has a total magnetic moment $\mu_T=\mu_A$ =2.0 μ_B/cell. This value is not the result of a transition from AF-to-FM interactions (the FM configuration would have $\mu_T=\mu_A$=4.0 μ_B/cell), but rather of a non-complete spin compensation. Indeed, the charge spin density plot (panel 5b) shows the cancellation of the magnetic moment of the central molecules (2-3). The comparison of the magnetic moment per atoms in the limiting cases for θ=0° and θ=20° (Figure S5) indicates an identical behaviour for external molecules 1-4, and the complete quenching of the magnetic moment, mostly on N atoms, of the two central molecules, which is a fingerprint of a local charge redistribution. As mentioned above, SOMO and SUMO are aromatic π states, delocalized over the entire molecules including nitrogen atoms. The close packed configuration of molecules 2 and 3, caused by the rotation, favours the π–π coupling, which results in the constructive hybridization of the molecular states, to form two new mixed delocalized orbitals across the film (Figure 5c). The intermolecular interaction changes the DOS plot of the system (panel d), where the external molecules (1-4) maintain their original spin-polarized character, while the internal layer gives rise to a spin-unpolarized peak that crosses the Fermi level (M-state in panel 5d and in the band structure of Figure S7b).

We have also considered the possible effects of structural changes (e.g., flattening of the molecules in the proximity of a substrate), which may quench the magnetic moment of the first layers. We changed the molecular arrangement of the bottom part of the 9 nm-thick film, by rotating only the lowest 4 molecules by 20°, 15°, 10° and 5°, respectively, to model the progressive readjustment of the molecules as expected in an experimental sample, because the interaction with the substrate plays a minor role with increasing the thickness, The results are

summarized in Figure 5e: the bottom 4 molecules rotate and flatten, similarly to the central layer of the 20° model discussed above (panel 5b); the remaining units stay in the θ=20° configuration, as in the thick film. The resulting system has μ_T=0.0 μ_B and μ_A =10.2 μ_B/cell where the rotated molecules have zero magnetic moment, while the rest maintains the AF interactions.

The modification of the magnetic properties caused by a different molecular arrangement is the key to understand the differences observed in the experimental results.

In light of this result, we have calculated the absorption at the nitrogen K-edge for two different angle orientation, 0° and 20°, averaged over the three directions of the incident radiation. We observe changes in the relative intensities of the lower energy features for the two different structures (Figure S8). In the case of the bulk-like molecular arrangement, the features are less intense, while they are more pronounced for the 20° configuration. This mirrors what we observe in the XAS experiment at PETRA III for the two different preparation conditions (Figure 3 and Figure S3), where the structure at lower photon energy is visible in the absorption curves measured for the films that show the presence of uncompensated spins

In the general case, depending on the growth conditions, the films may show magnetic interactions different from the AF, due to the presence of uncompensated spin layers, whose number (i.e., the final magnetization) depends on the specific different stacking (i.e., intermolecular π–π coupling). The molecules in the samples grown at 300 K have sufficient kinetic energy to mimic the bulk molecular arrangement, while in samples grown at a lower temperature the molecules assemble adopting a different orientation. This gives rise to a XMCD signal that stems from a spin unbalance in the molecular stack. Controlling the growth parameters influence thin film growth and their properties:[51] the substrate temperature during growth could be used as a tool to tune the magnetic character of purely organic thin films.

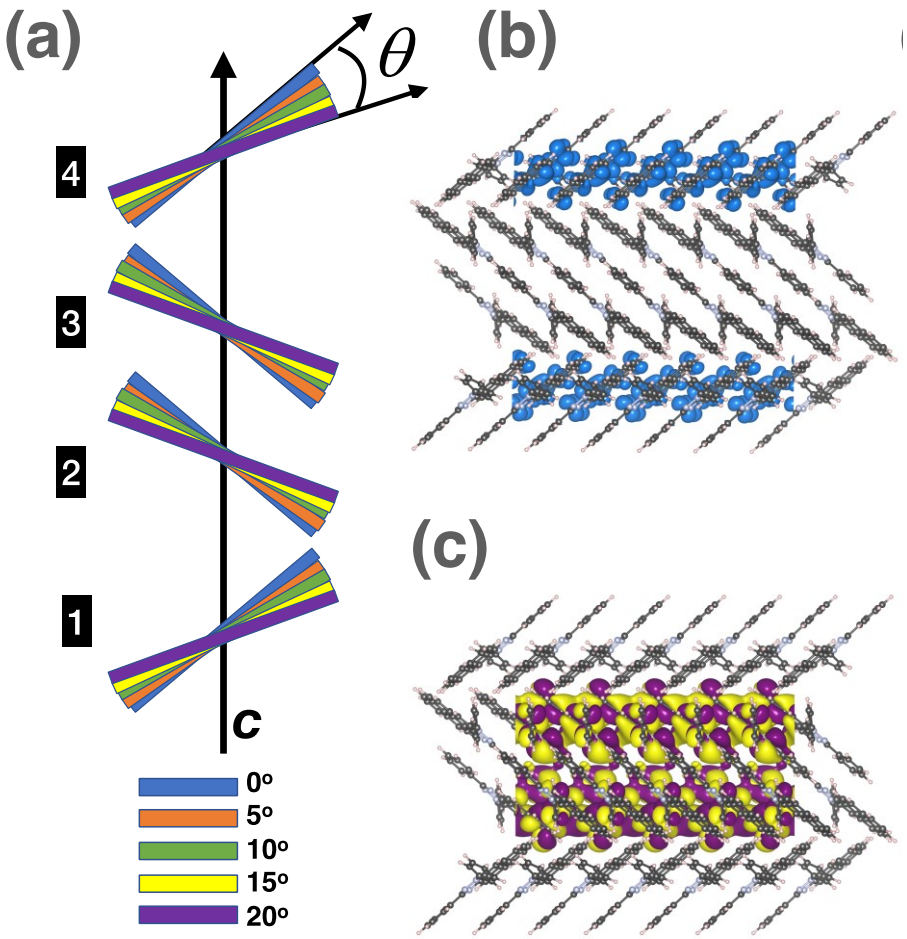
(a)
θ
4
3
2
1
c
0°
5°
10°
15°
20°
(b)
(c)

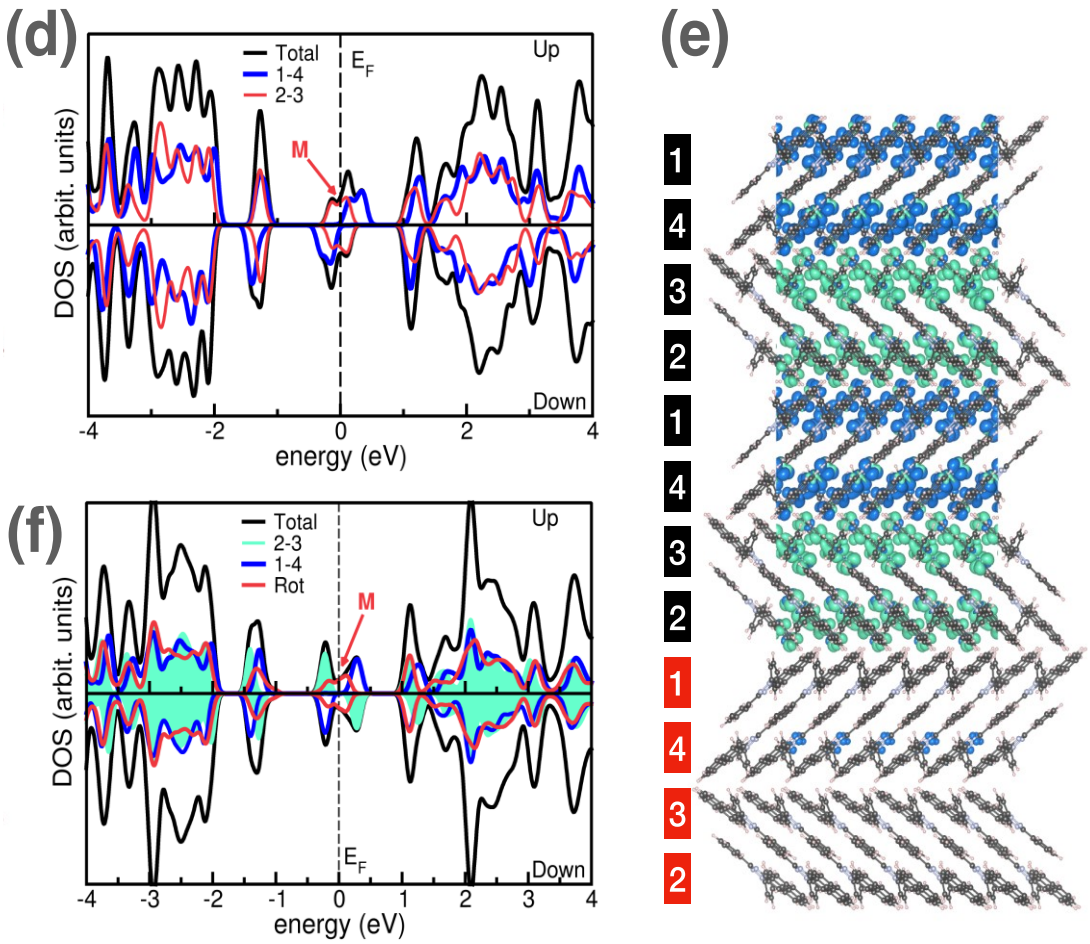

Figure 5. Calculation results for different molecular orientations in the Blatter-pyr films. **a.** Graphical model for a 3 nm-think film (4 molecules), rotated by angle θ with respect to the crystalline *c*-axis. Colors identify different rotation angles, θ=0° corresponds to the crystalline configuration (no rotation). **b.** Charge spin density plot of rotated model with θ =20°. **c.** Isosurface plot of the mixed M state and **d.** spin polarized DOS corresponding to the model in panel c. **e.** Side view and charge spin density plot for partially 9-nm thick film with a different molecular arrangement at the bottom. Red labels correspond to rotated molecules (20°, 15°, 10°, 5° for molecule 2, 3, 4, 1 respectively); black labels correspond to un-rotated stacked molecules. (f) Spin-polarized DOS corresponding to the structure in panel e). Red lines in panels c and f correspond to the projected DOS from spin-unpolarized molecules.

3. Conclusions

The use of soft X-rays spectroscopic techniques has revealed to be a powerful tool to acquire knowledge on thin films of purely organic radicals. For the first time, we showed that it is possible to investigate the magnetic character of purely organic radical thin films using XMCD. We measured the magnetic dichroism in thin films of purely organic radicals and found that the XMCD signature in the films is different than in the bulk depending on the film preparation. We explain this difference in terms of a different arrangement of the molecules in the two cases. We observed the presence of a layer of uncompensated spins that it is usually related to the presence of inorganic ferromagnetic/antiferromagnetic interfaces, and it is of interest for applications based on the polarisation and pinning of spins. This result further confirms the versality of purely organic radicals as potential candidates for new applications. In fact quantum technologies, breaking the taboo of working at very low temperatures, demonstrate that the reward is considerably high.

We emphasize that all spin and magnetic effects here reported are observed in a purely organic material. These are organic molecular systems that have been only very recently investigated in their film-phase, using a new approach, i.e., combining controlled evaporation and soft X-ray techniques in UHV.[14] Conversely, largely investigated thin film systems, such as thin films of phthalocyanines and porphyrins owe their magnetic properties to the presence of magnetic transition-metal ions, as in the case of single molecular magnets. [6,52-54]

The present work is only a first step in a largely unknown field. Many more experiments are needed to catch the intimate nature of magnetic ordering in radical thin films. Measuring the magnetization curves and the hysteresis loop versus the applied magnetic field to define a magnetic character, exploring a large set of preparation parameters and different radicals, including high-spin radical systems are the next necessary steps. New experimental approaches suitable for purely carbon-based materials are also necessary: we suggest that, from the

experimental point of view, in case of XAS at the absorption edges of light elements, measuring the clean substrate for minimizing the normalization issues might be beneficial. In fact, in near edge X-ray absorption fine structure (NEXAFS) spectroscopy the best way to normalize the curves at the absorption edge of thin films of light elements such as carbon is using the clean substrate signal rather than taking into account the total absorption of the beamline with a diode or a grid.[55] On the theoretical side, a model to interpret the XMCD results in this class of materials from a general point of view is missing.

The present work aims at stimulating a renewed discussion on the intimate meaning of magnetism in purely organic systems as well as at inspiring new experiments able to reveal the importance of synthetizing and manipulating stable radicals, to tune the collective magnetic behaviour of the thin films, also at higher temperatures.

METHODS

Experimental procedures. The molecules were synthetized as described in Ref.[17] Thin film were grown in UHV by using organic molecular beam deposition (OMBD). Native SiO_2 grown on single-side polished n-Si(111) wafers was used as the substrate for all thin films. The wafers were cleaned in an ultrasonic bath by immersion in ethanol and acetone for one hour each and annealed in ultra-high vacuum at around 500 K for several hours. The thin films were grown keeping the substrate temperature either at 290 or 300 K during deposition. When available, the cleanness of the substrates was checked by X-ray photoemission (XPS). The Knudsen cell was accurately calibrated, using a quartz microbalance and the XPS substrate signal attenuation, calculating the evaporation and the deposition rate, respectively, under the same conditions. The same cell was used during all experiments. The cell temperature during evaporation was 418 K, far below the onset of degradation of the radical as determined with thermal gravimetric

analysis.[17] The evaporation rate was 0.2 nm/min. Previously to the experiments discussed int this work, the films were characterized by using electron paramagnetic resonance to prove that the chosen evaporation conditions allow depositing films of intact radicals.[8,17] All measuring stations were equipped with preparations chambers that allowed installing the same calibrated Knudsen cells, therefore always using the same evaporation protocol. XPS measurements were performed in an UHV system consisting of a substrate preparation chamber, an OMBD-dedicated chamber, and an analysis chamber (base pressure 4 x 10^{-10} mbar) equipped with a SPECS Phoibos 150 hemispherical electron analyzer and a monochromatic Al Kα source (SPECS Focus 500). Further information on substrate preparation, film growth, stoichiometry measurements and fit calculations is given in Ref. [17].

UPS and XPS measurements were performed at the third-generation synchrotron radiation source Bessy II (Berlin, Germany) at the LowDose PES end-station, installed at the PM4 beamline ($E/\Delta E$=6000 at 400 eV) that included substrate preparation and film deposition facilities like those described above for the XPS station. The UPS measurements were carried out in single bunch mode with a SCIENTA ArTOF electron energy analyzer, the NEXAFS measurements in multibunch hybrid mode (ring current in top up mode=300 mA, c_{ff}=3, 100 μm exit slit).

The XMCD experimental setup[27] was installed at the XUV Beamlime P04 at the PETRA III synchrotron (Hamburg, Germany). At the Beamlime P04 each absorption edge could be scanned in a very short time, from few minutes to several seconds, and the beam exposure was minimized with a shutter. A magnetic field (± 7 T) was applied in the horizontal direction, collinear to the incoming photon beam. The measurements were carried out in normal incidence. Each element-resolved absorption curve was obtained averaging up to 54 scans, each measured on a fresh point on the film surface. All absorption spectra were recorded in total electron yield. To determine XMCD, the adsorption curves were divided by the incoming photon intensity current, I_0, measured with a photodiode, for the two polarizations. An offset was removed to

align the c+ and the c- curves, making sure that the pre-edge regions are equal. We subtracted the same linear background to the c+ and the c- curves and we normalized to have the same equal edge jump. The c- and c+ curves obtained in this way were subtracted to calculate XMCD.[32,33]

We have taken all precautions necessary to avoid radiation damage (e.g., short time beam exposure, shutter protection, defocusing of the beam, low dose radiation). All samples were carefully monitored for radiation damage during beam exposure. All measurements were performed on freshly prepared films.

Calculations. Calculations were performed with the Quantum Espresso Package[56,57] which implements a planewave formulation of the Density Functional Theory (DFT). Exchange-correlation was treated in the Perdew–Burke–Ernzerhof (PBE) Generalized Gradient Approximation (GGA)[58], and the spin degrees of freedom were described within the local spin-density approximation (LSDA). Tests on the effect of the exchange and correlation functional and the comparison with hybrids are reported in SI. Ionic potentials were described by using ab initio ultrasoft pseudopotentials of Vanderbilt's type.[59] Single-particle electronic wave functions (charge) were expanded in a plane-wave basis set up to an energy cutoff of 28 Ry (280 Ry). Van der Waals corrections (Grimme formulation[60]) to dispersive forces were included to improve the description of the intra- and inter-molecular interactions. A uniform (4x8x2) k-point mesh was used for sampling the 3D Brillouin zone of the bulk; a (4x8) k-point mesh was used for the 2D Brillouin zone of the films.

The molecular crystal was simulated by using periodic supercell. The initial structure was extracted by X-ray experimental data.

The Blatter-pyr 3D crystal was simulated in a monoclinic unitary cell of dimensions a= 13.65 Å, b=5.11 Å, c=28.24 Å, a=90.00°, b=99.47°, g=90.00°, which includes four molecules as shown in Figure 4 and Supporting Information (Figure S4). The films were modelled through periodically repeated monoclinic slabs, each including 12 Blatter-pyr radicals and a vacuum

layer (~1.5 nm) in the direction perpendicular to the surface plane, to avoid spurious interactions among the replicas. All structures were fully relaxed until forces on all atoms became lower than 0.03 eV/Å^{-1}.

NEXAFS spectra at the nitrogen K-edge were simulated by using the first-principles scheme based on the continued-fraction approach and ultrasoft pseudopotentials as implemented in the Quantum ESPRESSO package.[61] The reference 1s core level states were obtained by replacing the pseudopotential of a selected N atom with another one, which simulates the presence of a screened core hole. Since the molecule includes inequivalent nitrogen atoms, we repeated the NEXAFS calculations for each N atom of the radical and we averaged the resulting spectra. X-ray absorption spectra for each atom were also repeated changing the direction k_i of incident electric field along the three cartesian axes. The results are summarized in the SI.

Resource availability

Lead contact

Further information and requests for should be directed to and will be fulfilled by the lead contact, Maria Benedetta Casu (benedetta.casu@uni-tuebingen.de)

Materials availability

This study did not generate new unique materials.

Data and code availability

The datasets supporting the current study are available from the lead contact upon request.

SUPPLEMENTAL INFORMATION

Supplemental Information can be found online at

ACKNOWLEDGEMENTS

This paper is in memory of Wilfried Wurth. He was a brilliant scientist open to new ideas and views. We are deeply saddened that he will not see the result of our work because it was made possible also thanks to Wilfried's unprejudiced scientific approach. He would have appeared as a co-author.

The authors would like to thank Helmholtz-Zentrum Berlin (HZB) for providing beamtime at BESSY II (Berlin, Germany), and DESY (Hamburg, Germany), a member of the Helmholtz Association HGF, for the provision of experimental facilities at PETRA III, Tang Zahng, Moritz Hoesch, Kai Bagschik, Hilmar Adler, Elke Nadler and Sergio Naselli for technical support, Thomas Chassé for the access to the photoelectron spectroscopy lab at the University of Tübingen. We also thank Eberhard Goering for the XAS normalisation method. Financial support from HZB, DESY, and German Research Foundation (DFG) under the contract CA852/5-2 and CA852/11-1 is gratefully acknowledged. We thank the National Science Foundation (NSF), Chemistry Division for support of this research under Grants No. CHE-1665256 (A.R.) and CHE-1955349 (A.R.).

AUTHOR CONTRIBUTIONS

T.J., I.B., M.G., F.K., M.N., J.S., M.M. and M.B.C. took part in the beamtimes at PETRA III. M.G., F.C., E.G., R.O. and M.B.C. took part in the beamtimes at BESSY II. N.N.G. and A.R. designed and synthetized the radical. A.C. performed the calculations. M.B.C. conceived and supervised the project; interpreted the data and wrote the manuscript together with A.C. All authors contributed to the discussion and commented on the manuscript.

DECLARATION OF INTERESTS

The authors declare no competing interests.

Received:
Revised:
Accepted:
Published online:

REFERENCES

1. Slota, M., Keerthi, A., Myers, W.K., Tretyakov, E., Baumgarten, M., Ardavan, A., Sadeghi, H., Lambert, C.J., Narita, A., Müllen, K., and Bogani, L. (2018). Magnetic edge states and coherent manipulation of graphene nanoribbons. Nature *557*, 691-695. 10.1038/s41586-018-0154-7.
2. Sharpe, A.L., Fox, E.J., Barnard, A.W., Finney, J., Watanabe, K., Taniguchi, T., Kastner, M.A., and Goldhaber-Gordon, D. (2019). Emergent ferromagnetism near three-quarters filling in twisted bilayer graphene. Science *365*, 605-608. 10.1126/science.aaw3780.
3. Rajca, A., Wongsriratanakul, J., and Rajca, S. (2001). Magnetic Ordering in an Organic Polymer. Science *294*, 1503-1505. 10.1126/science.1065477.
4. Ohldag, H., Tyliszczak, T., Höhne, R., Spemann, D., Esquinazi, P., Ungureanu, M., and Butz, T. (2007). pi-Electron Ferromagnetism in Metal-Free Carbon Probed by Soft X-Ray Dichroism. Phys. Rev. Lett. *98*, 187204. 10.1103/PhysRevLett.98.187204.
5. Miller, J.S. (2011). Magnetically ordered molecule-based materials. Chem. Soc. Rev. *40*, 3266-3296. 10.1039/c0cs00166j.
6. Gatteschi, D., Sessoli, R., and Villain, J. (2006). Molecular Nanomagnets (Oxford University Press Inc.).
7. Tamura, M., Nakazawa, Y., Shiomi, D., Nozawa, K., Hosokoshi, Y., Ishikawa, M., Takahashi, M., and Kinoshita, M. (1991). Bulk ferromagnetism in the β-phase crystal of the p-nitrophenyl nitronyl nitroxide radical. Chem. Phys. Lett. *186*, 401-404.
8. Ciccullo, F., Calzolari, A., Bader, K., Neugebauer, P., Gallagher, N.M., Rajca, A., van Slageren, J., and Casu, M.B. (2019). Interfacing a Potential Purely Organic Molecular Quantum Bit with a Real-Life Surface. ACS Appl. Mater. Interfaces *11*, 1571-1578. 10.1021/acsami.8b16061.
9. Guo, H., Peng, Q., Chen, X.-K., Gu, Q., Dong, S., Evans, E.W., Gillett, A.J., Ai, X., Zhang, M., Credgington, D., et al. (2019). High stability and luminescence efficiency in donor–acceptor neutral radicals not following the Aufbau principle. Nat. Mater. *18*, 977-984. 10.1038/s41563-019-0433-1.
10. Ai, X., Evans, E.W., Dong, S., Gillett, A.J., Guo, H., Chen, Y., Hele, T.J.H., Friend, R.H., and Li, F. (2018). Efficient radical-based light-emitting diodes with doublet emission. Nature *563*, 536-540. 10.1038/s41586-018-0695-9.
11. Ji, Y., Long, L., and Zheng, Y. (2020). Recent advances of stable Blatter radicals: synthesis, properties and applications. Mater. Chem. Front. *4*, 3433-3443. 10.1039/D0QM00122H.
12. Wasielewski, M.R., Forbes, M.D.E., Frank, N.L., Kowalski, K., Scholes, G.D., Yuen-Zhou, J., Baldo, M.A., Freedman, D.E., Goldsmith, R.H., Goodson, T., et al. (2020). Exploiting chemistry and molecular systems for quantum information science. Nat. Rev. Chem. *4*, 490-504. 10.1038/s41570-020-0200-5.
13. Huang, Z., Zhang, Y., He, Y., Song, H., Yin, C., and Wu, K. (2017). A chemist's overview of surface electron spins. Chem. Soc. Rev. *46*, 1955-1976. 10.1039/C6CS00891G.
14. Casu, M.B. (2018). Nanoscale Studies of Organic Radicals: Surface, Interface, and Spinterface. Acc. Chem. Res. *51*, 753-760. 10.1021/acs.accounts.7b00612.
15. Zhang, Y., Zheng, Y., Zhou, H., Miao, M.-S., Wudl, F., and Nguyen, T.-Q. (2015). Temperature Tunable Self-Doping in Stable Diradicaloid Thin-Film Devices. Adv. Mater. *27*, 7412-7419. 10.1002/adma.201502404.

16. Mugnaini, V., Calzolari, A., Ovsyannikov, R., Vollmer, A., Gonidec, M., Alcon, I., Veciana, J., and Pedio, M. (2015). Looking Inside the Perchlorinated Trityl Radical/Metal Spinterface through Spectroscopy. J. Phys. Chem. Lett. *6*, 2101-2106. 10.1021/acs.jpclett.5b00848.
17. Ciccullo, F., Gallagher, N.M., Geladari, O., Chasse, T., Rajca, A., and Casu, M.B. (2016). A Derivative of the Blatter Radical as a Potential Metal-Free Magnet for Stable Thin Films and Interfaces. ACS Appl. Mater. Interfaces *8*, 1805–1812.
18. Stöhr, J. (1999). Exploring the microscopic origin of magnetic anisotropies with X-ray magnetic circular dichroism (XMCD) spectroscopy. J. Magn. Magn. Mater. *200*, 470-497. https://doi.org/10.1016/S0304-8853(99)00407-2.
19. Brune, H., and Gambardella, P. (2009). Magnetism of individual atoms adsorbed on surfaces. Surf. Sci. *603*, 1812-1830. https://doi.org/10.1016/j.susc.2008.11.055.
20. Cornia, A., Talham, D.R., and Affronte, M. (2016). Thin Layers of Molecular Magnets. In Molecular Magnetic Materials, pp. 187-229. 10.1002/9783527694228.ch8.
21. Schütz, G., Wagner, W., Wilhelm, W., Kienle, P., Zeller, R., Frahm, R., and Materlik, G. (1987). Absorption of circularly polarized x rays in iron. Phys. Rev. Lett. *58*, 737-740. 10.1103/PhysRevLett.58.737.
22. Savu, S.-A., Biswas, I., Sorace, L., Mannini, M., Rovai, D., Caneschi, A., Chassé, T., and Casu, M.B. (2013). Nanoscale Assembly of Paramagnetic Organic Radicals on Au(111) Single Crystals. Chem.-Eur. J. *19*, 3445-3450. 10.1002/chem.201203247.
23. Blundell, S.J., and Pratt, F.L. (2004). Organic and molecular magnets. Journal of Physics: Condensed Matter *16*, R771-R828. 10.1088/0953-8984/16/24/r03.
24. Deumal, M., Vela, S., Fumanal, M., Ribas-Arino, J., and Novoa, J.J. (2021). Insights into the magnetism and phase transitions of organic radical-based materials. Journal of Materials Chemistry C *9*, 10624-10646. 10.1039/D1TC01376A.
25. Blatter, H.M., and Lukaszewski, H. (1968). A new stable free radical. Tetrahedron Lett. *9*, 2701-2705. http://dx.doi.org/10.1016/S0040-4039(00)89678-1.
26. Constantinides, C.P., Koutentis, P.A., Krassos, H., Rawson, J.M., and Tasiopoulos, A.J. (2011). Characterization and Magnetic Properties of a "Super Stable" Radical 1,3-Diphenyl-7-trifluoromethyl-1,4-dihydro-1,2,4-benzotriazin-4-yl. J. Org. Chem. *76*, 2798-2806. 10.1021/jo200210s.
27. Beeck, T., Baev, I., Gieschen, S., Meyer, H., Meyer, S., Palutke, S., Feulner, P., Uhlig, K., Martins, M., and Wurth, W. (2016). New experimental perspectives for soft x-ray absorption spectroscopies at ultra-low temperatures below 50 mK and in high magnetic fields up to 7 T. Rev. Sci. Instrum. *87*, 045116. 10.1063/1.4947516.
28. Zheng, Y., Miao, M.-s., Kemei, M.C., Seshadri, R., and Wudl, F. (2014). The Pyreno-Triazinyl Radical – Magnetic and Sensor Properties. Isr. J. Chem. *54*, 774-778. 10.1002/ijch.201400034.
29. Ohldag, H., Scholl, A., Nolting, F., Arenholz, E., Maat, S., Young, A.T., Carey, M., and Stöhr, J. (2003). Correlation between Exchange Bias and Pinned Interfacial Spins. Phys Rev Lett *91*, 017203. 10.1103/PhysRevLett.91.017203.
30. Nogués, J., and Schuller, I.K. (1999). Exchange bias. J. Magn. Magn. Mater. *192*, 203-232. https://doi.org/10.1016/S0304-8853(98)00266-2.
31. Berkowitz, A.E., and Takano, K. (1999). Exchange anisotropy — a review. J. Magn. Magn. Mater. *200*, 552-570. https://doi.org/10.1016/S0304-8853(99)00453-9.
32. Goering, E., Fuss, A., Weber, W., Will, J., and Schütz, G. (2000). Element specific x-ray magnetic circular dichroism magnetization curves using total electron yield. J. Appl. Phys. *88*, 5920-5923. 10.1063/1.1308095.
33. Goering, E., Gold, S., Bayer, A., and Schuetz, G. (2001). Non-symmetric influences in the total electron yield X-ray magnetic circular dichroism signal in applied magnetic fields. J. Synchrotron Rad. *8*, 434-436. 10.1107/s0909049500018343.
34. Lodi Rizzini, A., Krull, C., Balashov, T., Mugarza, A., Nistor, C., Yakhou, F., Sessi, V., Klyatskaya, S., Ruben, M., Stepanow, S., and Gambardella, P. (2012). Exchange Biasing Single Molecule

Magnets: Coupling of TbPc2 to Antiferromagnetic Layers. Nano Letters *12*, 5703-5707. 10.1021/nl302918d.
35. Wang, Y.Y., Song, C., Wang, G.Y., Zeng, F., and Pan, F. (2014). Evidence for asymmetric rotation of spins in antiferromagnetic exchange-spring. New Journal of Physics *16*, 123032. 10.1088/1367-2630/16/12/123032.
36. Donges, A., Khmelevskyi, S., Deak, A., Abrudan, R.-M., Schmitz, D., Radu, I., Radu, F., Szunyogh, L., and Nowak, U. (2017). Magnetization compensation and spin reorientation transition in ferrimagnetic ${\mathrm{DyCo}}_{5}$: Multiscale modeling and element-specific measurements. Physical Review B *96*, 024412. 10.1103/PhysRevB.96.024412.
37. Nistor, C., Krull, C., Mugarza, A., Stepanow, S., Stamm, C., Soares, M., Klyatskaya, S., Ruben, M., and Gambardella, P. (2015). Exchange bias of ${\mathrm{TbPc}}_{2}$ molecular magnets on antiferromagnetic FeMn and ferromagnetic Fe films. Physical Review B *92*, 184402. 10.1103/PhysRevB.92.184402.
38. Duhm, S., Heimel, G., Salzmann, I., Glowatzki, H., Johnson, R.L., Vollmer, A., Rabe, J.P., and Koch, N. (2008). Orientation-dependent ionization energies and interface dipoles in ordered molecular assemblies. Nat. Mater. *7*, 326-332. 10.1038/nmat2119.
39. Klett, B., Cocchi, C., Pithan, L., Kowarik, S., and Draxl, C. (2016). Polymorphism in α-sexithiophene crystals: relative stability and transition path. Phys. Chem. Chem. Phys. *18*, 14603-14609. 10.1039/C6CP01405D.
40. Jones, A.O.F., Chattopadhyay, B., Geerts, Y.H., and Resel, R. (2016). Substrate-Induced and Thin-Film Phases: Polymorphism of Organic Materials on Surfaces. Adv. Funct. Mater. *26*, 2233–2255. 10.1002/adfm.201503169.
41. Poulopoulos, P., and Baberschke, K. (1999). Magnetism in thin films. J. Phys. Condens. Matter *11*, 9495-9515. 10.1088/0953-8984/11/48/310.
42. Mori, T. (2016). Electronic Properties of Organic Conductors (Springer Japan).
43. Kowarik, S., Gerlach, A., Sellner, S., Schreiber, F., Cavalcanti, L., and Konovalov, O. (2006). Real-Time Observation of Structural and Orientational Transitions during Growth of Organic Thin Films. Physical Review Letters *96*, 125504. 10.1103/PhysRevLett.96.125504.
44. Dalal, S.S., Walters, D.M., Lyubimov, I., de Pablo, J.J., and Ediger, M.D. (2015). Tunable molecular orientation and elevated thermal stability of vapor-deposited organic semiconductors. Proceedings of the National Academy of Sciences *112*, 4227-4232. 10.1073/pnas.1421042112.
45. Kowarik, S., Gerlach, A., and Schreiber, F. (2008). Organic molecular beam deposition: fundamentals, growth dynamics, andin situstudies. Journal of Physics: Condensed Matter *20*, 184005. 10.1088/0953-8984/20/18/184005.
46. Constantinides, C.P., Koutentis, P.A., and Rawson, J.M. (2012). Antiferromagnetic Interactions in 1D Heisenberg Linear Chains of 7-(4-Fluorophenyl) and 7-Phenyl-Substituted 1,3-Diphenyl-1,4-dihydro- 1,2,4-benzotriazin-4-yl Radicals. Chemistry – A European Journal *18*, 15433-15438. 10.1002/chem.201202784.
47. The use of a higher level of theory, such as hybrid exchange-correlation (XC) functional does not change this picture. Preliminary tests on the single molecule show that the inclusion of B3LYP functional barely opens the energy gap between the SOMO and SUMO molecular orbitals, while it does not modify the symmetry or the order of the single molecular orbitals.
48. Casu, M.B., Scholl, A., Bauchspiess, K.R., Hubner, D., Schmidt, T., Heske, C., and Umbach, E. (2009). Nucleation in Organic Thin Film Growth: Perylene on Al2O3/Ni3Al(111). J. Phys. Chem. C *113*, 10990-10996. 10.1021/jp809497h.
49. Schreiber, F. (2004). Organic molecular beam deposition: Growth studies beyond the first monolayer. physica status solidi (a) *201*, 1037-1054. https://doi.org/10.1002/pssa.200404334.
50. Witte, G., and Wöll, C. (2011). Growth of aromatic molecules on solid substrates for applications in organic electronics. Journal of Materials Research *19*, 1889-1916. 10.1557/JMR.2004.0251.

51. Forrest, S.R. (1997). Ultrathin Organic Films Grown by Organic Molecular Beam Deposition and Related Techniques. Chem. Rev. *97*, 1793-1896. 10.1021/cr941014o.
52. Coronado, E. (2020). Molecular magnetism: from chemical design to spin control in molecules, materials and devices. Nat. Rev. Mater. *5*, 87-104. 10.1038/s41578-019-0146-8.
53. Cinchetti, M., Dediu, V.A., and Hueso, L.E. (2017). Activating the molecular spinterface. Nature Materials *16*, 507. 10.1038/nmat4902.
54. Gruber, M., Ibrahim, F., Boukari, S., Isshiki, H., Joly, L., Peter, M., Studniarek, M., Da Costa, V., Jabbar, H., Davesne, V., et al. (2015). Exchange bias and room-temperature magnetic order in molecular layers. Nature Materials *14*, 981-984. 10.1038/nmat4361.
55. Schöll, A., Zou, Y., Schmidt, T., Fink, R., and Umbach, E. (2003). Energy calibration and intensity normalization in high-resolution NEXAFS spectroscopy. J. Electron. Spectros. Relat. Phenomena *129*, 1-8. https://doi.org/10.1016/S0368-2048(03)00016-1.
56. Giannozzi, P., Andreussi, O., Brumme, T., Bunau, O., Buongiorno Nardelli, M., Calandra, M., Car, R., Cavazzoni, C., Ceresoli, D., Cococcioni, M., et al. (2017). Advanced capabilities for materials modelling with Quantum ESPRESSO. J. Condens. Matter Phys. *29*, 465901. 10.1088/1361-648x/aa8f79.
57. Giannozzi, P., Baroni, S., Bonini, N., Calandra, M., Car, R., Cavazzoni, C., Ceresoli, D., Chiarotti, G.L., Cococcioni, M., Dabo, I., et al. (2009). QUANTUM ESPRESSO: a modular and open-source software project for quantum simulations of materials. J. Phys. Condens. Matter *21*, 395502.
58. Perdew, J.P., Burke, K., and Ernzerhof, M. (1996). Generalized Gradient Approximation Made Simple. Phys. Rev. Lett. *77*, 3865-3868.
59. Vanderbilt, D. (1990). Soft self-consistent pseudopotentials in a generalized eigenvalue formalism. Phys. Rev. B *41*, 7892-7895.
60. Grimme, S. (2006). Semiempirical GGA‐type density functional constructed with a long‐range dispersion correction. J. Comput. Chem. *27*, 1787-1799. doi:10.1002/jcc.20495.
61. Gougoussis, C., Calandra, M., Seitsonen, A.P., and Mauri, F. (2009). First-principles calculations of x-ray absorption in a scheme based on ultrasoft pseudopotentials: From alpha-quartz to high-Tc compounds. Phys. Rev. B *80*, 075102. 10.1103/PhysRevB.80.075102.